RSC Advances

PAPER

Cite this: *RSC Adv.*, 2024, **14**, 19284

Impact of BSA and Au^{3+} concentration on the formation and fluorescence properties of Au nanoclusters†

Tao Li,‡[a] Zhuo Li,‡[a] Fengjiao Chen,[b] Liying Zhu,[c] Hua Tang,[a] Dan Wang*[d] and Zhenrong Tang*[e]

Bovine serum albumin-stabilized Au nanoclusters (BSA-Au NCs) have emerged as promising contenders for imaging agents and highly sensitive fluorescence sensors due to their biocompatibility and strong photoluminescence. Optimizing the synthesis conditions of BSA-Au NCs is crucial for enhancing fluorescence imaging and other nanocluster applications. In this study, for the first time, we systematically investigated the effects of BSA concentration and Au^{3+} on both particle size and optical characteristics of BSA-Au NCs. When the two components achieved a suitable concentration ratio, it was beneficial to form BSA-Au NCs with a high quantum yield (QY = 74.30%) and good fluorescence stability. In contrast, an inappropriate concentration ratio would lead to the formation of gold nanoparticles (Au NPs), and their internal filtration effect (IFE) would attenuate the fluorescence emission of BSA-Au NCs. The BSA-Au NCs were then employed as efficient fluorescence sensors for detecting Hg^{2+}. Furthermore, the growth mechanism of BSA-Au NCs was elucidated by monitoring fluorescence changes during different incubation times. The BSA-Au NCs with a high quantum yield introduce a novel synthetic concept for sensitive fluorescent probes and expanding versatile applications of BSA-Au NCs in catalysis, chemical sensing and biomedicine.

Received 14th February 2024
Accepted 10th June 2024

DOI: 10.1039/d4ra01140f

rsc.li/rsc-advances

Introduction

Recently, preparation and modification of nanomaterial-based diagnostics and therapeutics have become an emerging field in clinical research.[1] Gold nanoclusters (Au NCs) have attracted extensive attention due to their discrete electronic energy levels, large Stokes shifts and size-dependent fluorescence.[2–4] Au NCs, also known as gold nanoaggregates, are composed of multiple to hundreds of gold atoms and have a size smaller than 2 nm, which is comparable to the Fermi wavelength of metallic conduction electrons, resulting in molecule-like properties.[5,6] These Au NCs typically have a core–shell structure, consisting of gold core and surface ligand.[7] The ligands commonly used encompass thiols, peptides, proteins, nucleic acid chains, dendrimers, and others.[8–10] Among them, protein-stabilized Au NCs synthesized through hydrothermal green methods have under spotlight due to their favorable biocompatibility, stability, easy of modification, and resistance to photobleaching.[11,12] Bovine serum albumin (BSA) contains 35 cysteine residues and 20 tyrosine groups, which not only provides an ample supply of –SH groups for the attachment of Au^{3+}, but also enable the complete reduction of Au^{3+}.[3,13–15] Serving as an effective reducing agent, BSA preserves the fluorescence and structural stability of Au NCs while preventing the aggregation of gold nuclei.[16] Furthermore, BSA acts as an "environmental friendliness" raw material, which not only regulates the surface chemical properties of Au NCs but also mitigates their potential toxicity.[17] Consequently, BSA-Au NCs exhibit promising prospects for various applications such as bioimaging and analysis, drug delivery, targeted diagnosis and therapy, nanoenzyme catalysis and environmental monitoring.[18–20]

The previous researches have indicated that the quantum yield of BSA-Au NCs are mostly ranging from 0.1% to 40%, and predominantly emits red light with inconsistent particle sizes, which significantly hinder the development and application of Au NCs.[6,21] In order to achieve Au NCs with desirable characteristics such as high quantum yield, particle size uniformity and well stability, it is imperative to further investigate the synthesis conditions. The synthesis of BSA-Au NCs is influenced

[a]*Key Laboratory of Molecular Biology for Infectious Diseases (Ministry of Education), Chongqing Medical University, Chongqing, China*
[b]*Department of Clinical Laboratory, The First Affiliated Hospital of Chongqing Medical University, Chongqing, China*
[c]*Center for Clinical Laboratories, The Affiliated Hospital of Guizhou Medical University, Guiyang, China*
[d]*Post-Doctoral Research Center, The People's Hospital of Rongchang District, Chongqing, China. E-mail: cqwangdan61@163.com*
[e]*Department of Breast and Thyroid Surgery, The First Affiliated Hospital of Chongqing Medical University, Chongqing, China. E-mail: tangzhenrong1992@163.com*

† Electronic supplementary information (ESI) available. See DOI: https://doi.org/10.1039/d4ra01140f

‡ Tao Li and Zhuo Li contributed equally to this work.

by various factors, such as pH,[22] temperature,[6,23] incubation time[24] and raw material concentration. Chen *et al.* successfully prepared Au NC_S by reducing Au^{3+} with papain and found that various concentrations of papain influenced the red emission of Au NCs.[18] Yang *et al.* found that the nitrogen dopant content in the raw materials had a substantial impact on the optical properties of graphene quantum dots (GQD).[25] Xavier *et al.* synthesized Au NCs using lactoferrin as a reductant and observed varying red emission intensities of the Au NCs by manipulating the concentration levels of lactoferrin and Au^{3+}.[26] Hence, it was hypothesized that the concentration level and ratio of BSA and Au^{3+} exert notable influences on the particle size, fluorescence properties, and stability of BSA-Au NCs. However, none of these studies have comprehensively elucidated how the concentration and ratio of raw materials affect the formation and optical properties of BSA-Au NCs.

In this work, we had systematically revealed that the optical properties and particle size of Au NCs were related to the concentration level and concentration ratio of BSA to Au^{3+} for the first time. Specifically, only the appropriate concentration ratio could form BSA-Au NCs with uniform size, good stability and excellent quantum yield (QY = 74.3%). It was also observed that the inner filter effect (IFE) of Au NPs in the solution, suggesting that the fluorescence spectrum of the solution couldn't accurately represent the true characteristics of the synthesized Au NCs. The impact of raw material concentration on the growth of Au NCs was further explored by monitoring the alterations in fluorescence spectra across different synthesis systems. In addition, the BSA-Au NCs could be used as efficient fluorescence sensors for the sensitive and selective detection of Hg^{2+} (Scheme 1).

Experimental

Materials and reagents

Chloroauric acid tetrahydrate ($HAuCl_4 \cdot 4H_2O$) and sodium hydroxide (NaOH) were supplied from Sinopharm Chemical Reagent Co., Ltd (Shanghai, China). Bovine serum albumin (BSA) was purchased from Dalian Meilun Biotech Co., Ltd. 30% acrylamide (acrylamide/bisacylamide = 29 : 1), ammonium persulfate (APS), 1 M Tris–HCl (pH 8.8), 1 M Tris–HCl (pH 6.8), and trypsin (activity ≥ 180 U per mg protein) were bought from Sangon Biotech Co., Ltd (Shanghai, China). Phosphate buffer saline (PBS) was supplied by Thermo Fisher Scientific (Wilmington, USA). *N*,*N*,*N*′,*N*′-tetramethylethylenediamine (TEMED), citrate and tannic acid, potassium chloride (KCl), nickel(II) chloride hexahydrate ($NiCl_2 \cdot 6H_2O$), iron(III) chloride hexahydrate ($FeCl_3 \cdot 6H_2O$), iron(II) chloride tetrahydrate ($FeCl_2 \cdot 4H_2O$), stannous chloride dihydrate ($SnCl_2 \cdot 2H_2O$), aluminum chloride hexahydrate ($AlCl_3 \cdot 6H_2O$), chromic chloride hexahydrate ($CrCl_3 \cdot 6H_2O$), magnesium chloride hexahydrate ($MgCl_2 \cdot 6H_2O$), zinc nitrate ($Zn(NO_3)_2$), manganese(II) chloride tetrahydrate ($MnCl_2 \cdot 4H_2O$), mercuric nitrate monohydrate ($Hg(NO_3)_2 \cdot H_2O$) were purchased from Shanghai Aladdin Biochemical Technology Co., Ltd. Coomassie blue stain solution and corresponding destaining solution were purchased from Beijing Leagene Biotech. Co., Ltd. The reagents and chemicals used were analytical reagent grade and used directly without further purification. Millipore Milli-Q gradient ultrapure water system (Millipore, MA) was used to prepare ultrapure water throughout the experiments.

Apparatus

The fluorescence spectra of the products were recorded by a F-4700 Fluorescence Spectrophotometer (HITACHI, Tokyo, Japan). Ultraviolet-visible (UV-vis) spectra of BSA-Au NCs were obtained using a Double Beam Spectrophotometer UH5300 (HITACHI, Tokyo, Japan). BSA-Au NCs was imaged on an OI600 MF Multifunction Imager (Bio-OI, Guangzhou, China). Native polyacrylamide gel electrophoresis (Native-PAGE) was performed on a DYY-6C electrophoresis analyzer (Liu Yi Instrument Company, China). BSA-Au NCs mixed in polyacrylamide gel were identified by Bio-Rad ChemDoc XRS (Bio-Rad, USA). The high-resolution transmission electron microscope

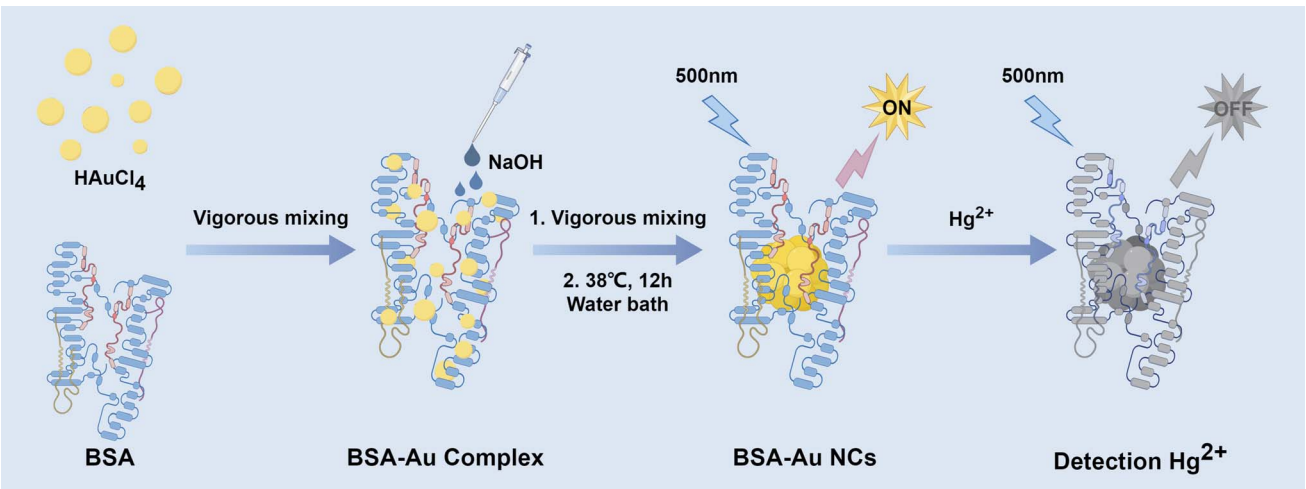

Scheme 1 Schematic representation of the synthesis and Hg^{2+} detection of BSA-Au NCs.

(HRTEM, FEI Tecnai G2 F30, USA) was used to characterize the size and morphology of the BSA-Au NCs and Au NPs. Molecular weight distribution of BSA-Au NCs were analyzed by Gel Permeation Chromatography (GPC, LC20AT, Shimadzu, Japan). X-ray photoelectron spectroscopy (XPS) was performed to explore the electronic structures of the BSA-Au NCs on a Thermo Scientific Escalab 250XI XPS instrument. The XPS spectra of the Au 4f core levels were deconvolved using the AVANTAGE software (Version 5.9922). The sp^3 C 1s peak was used as a reference for the binding energy calibration.

Synthesis of BSA-Au NCs

The synthesis of BSA-Au NCs was optimized with reference to the previous study reported by Xie *et al.*[6] Briefly: $HAuCl_4$ solution (1 mL) was added to BSA solution (1 mL) and stirred vigorously for 7 min. NaOH (1 M) was added to make the solution pH = 12 to activate the reducing ability of BSA and further stirred vigorously for 3 min. Finally, the reaction was terminated by incubation for 12 h at 38 °C. The obtained BSA-Au NCs compounds were stored at 4 °C for further use.

Synthesis of Au NPs

Citrate-capped Au NPs were synthesized by an improved reduction method of citric/tannic acid.[27] Aqueous solutions of $HAuCl_4$ were prepared firstly (25 mL, 25 mM). The sodium citrate solution (15 mL, 2.2 mM) and tannic acid solution (0.01 mL, 2.5 mM) were mixed in a conical flask and stirred vigorously for 10 min at 70 °C. Then $HAuCl_4$ aqueous solution was added and performed at 70 °C for 10 min. The products were cooled to room temperature and dialyzed with deionized water before storing at 4 °C.

Hg^{2+} detection using BSA-Au NCs

First, we dialyzed BSA-Au NCs for 6 h. For sensitivity testing, BSA-Au NCs (0.5 mL, diluted 40 times) were mixed with various concentrations of Hg^{2+} solution (0.5 mL, 0.01 μM to 100 μM). For specificity testing, BSA-Au NCs (0.5 mL, diluted 10 times) were mixed with different metal ion solutions (0.5 mL, 40 μM). The solutions were kept at room temperature for 5 min before detection, and then detect the fluorescence at 650 nm. Notably, all tests are conducted under room temperature conditions.

Native-PAGE

BSA-Au NCs were concentrated by 10% Native-PAGE at a constant voltage of 110 V for 20 min, and then converted to a voltage of 160 V for 60 min for separation gel electrophoresis. The whole experiment was going on at 4 °C.

Results and discussion

The effect of different concentration level of the reaction system on the synthesize of Au NCs

Previous studies had consistently maintained a concentration ratio of 14.71 : 1 for BSA to Au^{3+}.[22,28,29] In this study, we initially examined the influence of BSA and Au^{3+} concentration levels on the formation of Au NCs and their corresponding emission properties (Fig. 1a). As the concentration increased, the solution transitioned from colorless to orange-brown, indicating the gradual formation of the Au NCs or Au NPs. These synthetic products exhibited a progressive augmentation of red fluorescence under 365 nm excitation light (Fig. 1b). Emission spectra of BSA treated with/without NaOH were shown as control groups. Notably, the blue fluorescence (~400 nm) emitted by the products synthesized using low concentration raw materials (Groups 1–3) surpassed the autofluorescence of the control groups, indicating the existence of small nanoclusters (*e.g.*, Au_5 NCs[14]). As the concentration of BSA and Au^{3+} escalated, the blue fluorescence exhibited a gradual decline, while the red fluorescence intensified, indicating an augmentation in the quantity of larger Au NCs (*e.g.*, Au_{25} NCs[30]) (Fig. 1c and d). The fluorescence lifetime of blue light in Groups 1–4 was nanosecond scale, and the fluorescence lifetime of red light was microsecond scale. When excited at 338 nm, the PL lifetime increased gradually with the increase of the concentration level of raw materials, and changed from 3.40 to 15.36 ns. The fluorescence lifetime of red fluorescence was similar (Fig. S1†). The XPS analysis revealed that the small Au NCs were composed of Au^0, while the presence of Au^+ coexisted with Au^0 in the larger Au NCs (Fig. S2†). Previous studies have demonstrated that the gold cores of the Au_5 form exclusively consist of Au^0, whereas the gold cores of the Au_{25} form consisted of both Au^0 and Au^+.[28,29] The higher peaks observed in the Au $4f_{5/2}$ and Au $4f_{7/2}$ spectra could be attributed to the reduction of Au^0 by BSA, while the lower peaks correspond to the presence of Au^+.[31] This finding suggested that BSA facilitated the reduction of Au^{3+} to both Au^0 and Au^+, leading to the growth and formation of Au NCs. The UV-vis spectra analysis indicated that Group 1 and Group 2 did not exhibit any distinctive absorption peak when compared to the control groups. However, Group 3 and Group 4 displayed a significant absorbance at approximately 520 nm, which is indicative of the presence of BSA-Au complexes with diameters exceeding 2 nm (Fig. 1e). This feature is consistent with localized surface plasmon resonance (LSPR). HRTEM results showed that the average size of the Au NCs increased from 1.50 to 4.39 nm, which was consistent with the spectral results (Fig. 1f–i).

Native-PAGE verified the presence of BSA oligomers in addition to the prominent 66 kDa band, which corresponds to the molecular weight of BSA protein. The introduction of NaOH was found to disrupt the BSA structure and impede the electrophoretic mobility of protein. Furthermore, the electrophoretic mobility of Au NCs exhibited deceleration as the concentration level increased (Fig. 1j). Fluorescence emitted was also observed when subjected to 365 nm excitation, suggesting that both monomers and oligomers of BSA could serve as ligands to stabilize Au NCs (Fig. 1k). The results of electrophoresis were consistent with the results of HRTEM, indicating that the Native-PAGE could be used as a useful tool to characterize the molecular weight of Au NCs for subsequent experimental studies. Additionally, the molecular weight distribution of BSA-Au NCs was verified through gel permeation chromatography (GPC). Fig. 1l illustrated that the higher the

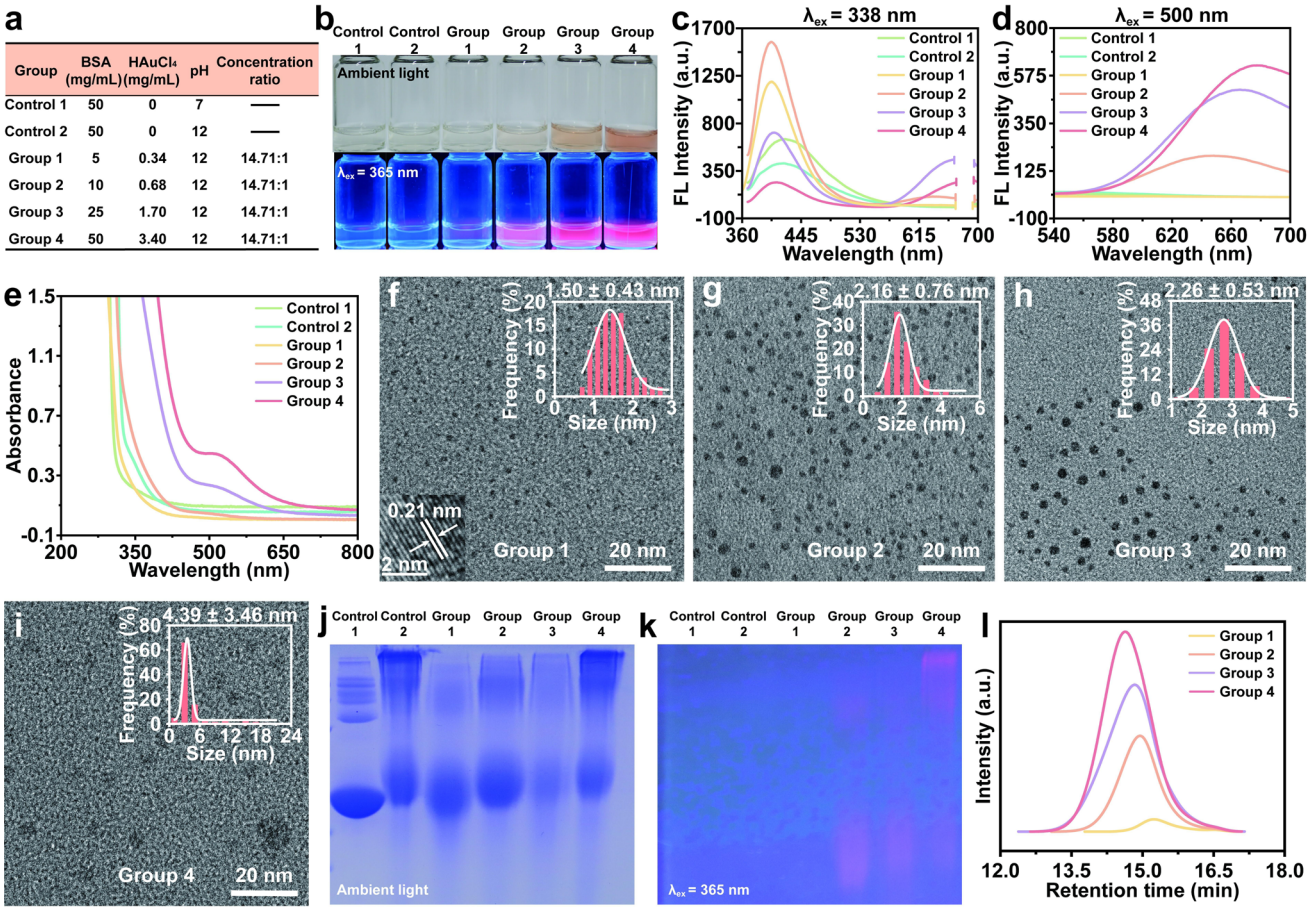

Fig. 1 The effect of various concentration level of the reaction system on the synthesize of BSA-Au NCs, while maintaining a fixed concentration ratio. (a) The various concentration levels of the reaction system in a fixed ratio. (b) Digital images of each group under ambient (above) and 365 nm ultraviolet lamp (below). (c and d) Photoemission spectra of each group (λ_{ex} = 338 nm and 500 nm). (e) UV-vis absorption spectrum of each group. (f–i) The HRTEM images and particle size (inset) of BSA-Au NCs. (j) Coomassie brilliant blue staining gel image. (k) Native-PAGE under 365 nm ultraviolet lamp. (l) GPC trace of BSA-Au NCs. All photoemission spectra were slit widths of excitation: 5 nm, slit widths of emission: 5 nm, and voltage: 600 V.

concentration level, the greater the molecular weight of BSA-Au NCs. These results suggested the concentration levels of the raw materials affected the size and optical properties of Au NCs.

The formation of BSA oligomer-stabilized Au NCs

It was hypothesized that the presence of oligomer-stabilized Au NCs contributed to the inadequate uniformity of NCs (Fig. S3†). Therefore, varying concentrations of trypsin were employed to digest BSA oligomers (Fig. 2a). BSA oligomers were almost digested by 0.08 mg mL^{-1} trypsin and then used to synthesize Au NCs. The presence of BSA-stabilized Au NCs after trypsin treatment did not affect the fluorescence spectral changes of the solution (Fig. 2b–d). Interestingly, we found that the red fluorescence from BSA oligomer-stabilized Au NCs was still visible, indicating that the oligomers formed by BSA itself are not the only reason for the formation of BSA oligomer-stabilized Au NCs (Fig. 2e). According to previous studies,[32] we proposed a second conjecture on the formation of BSA oligomer-stabilized Au NCs: multiple BSA monomers stabilized an Au NC with a free cysteine residue. To investigate this, we employed EDTA-2Na, the known chelators of Au^{3+}, to impede the formation of Au NCs (Fig. 2f). A large amount of Au^{3+} was chelated when using high concentrations of EDTA-2Na, resulting in the disappearance of large Au NCs and the formation of small Au NCs (Fig. 2g–i). Native-PAGE analysis indicated that the concentration of EDTA-2Na did not have a significant effect on the presence of BSA oligomer-stabilized Au NCs, suggesting that the formation of BSA oligomer-stabilized Au NCs was not influenced by the presence of Au NCs (Fig. 2j). Under alkaline conditions, the structure of BSA will change, and at pH > 10, it will change to an "A" conformation. In this conformation, domain I and domain III are fully unfolded, exposing the internal cysteine residues. The oxidation of sulfhydryl groups in amino acids and the cross-linking between disulfide bonds promoted the formation of clusters.[24,33] In light of this, we conducted experiments by adding varying volumes of NaOH (1 M) to a BSA solution and observed an increase in oligomer formation with increasing NaOH concentration (Fig. 2k). These findings suggested that an alkaline environment promoted the formation of BSA oligomer-

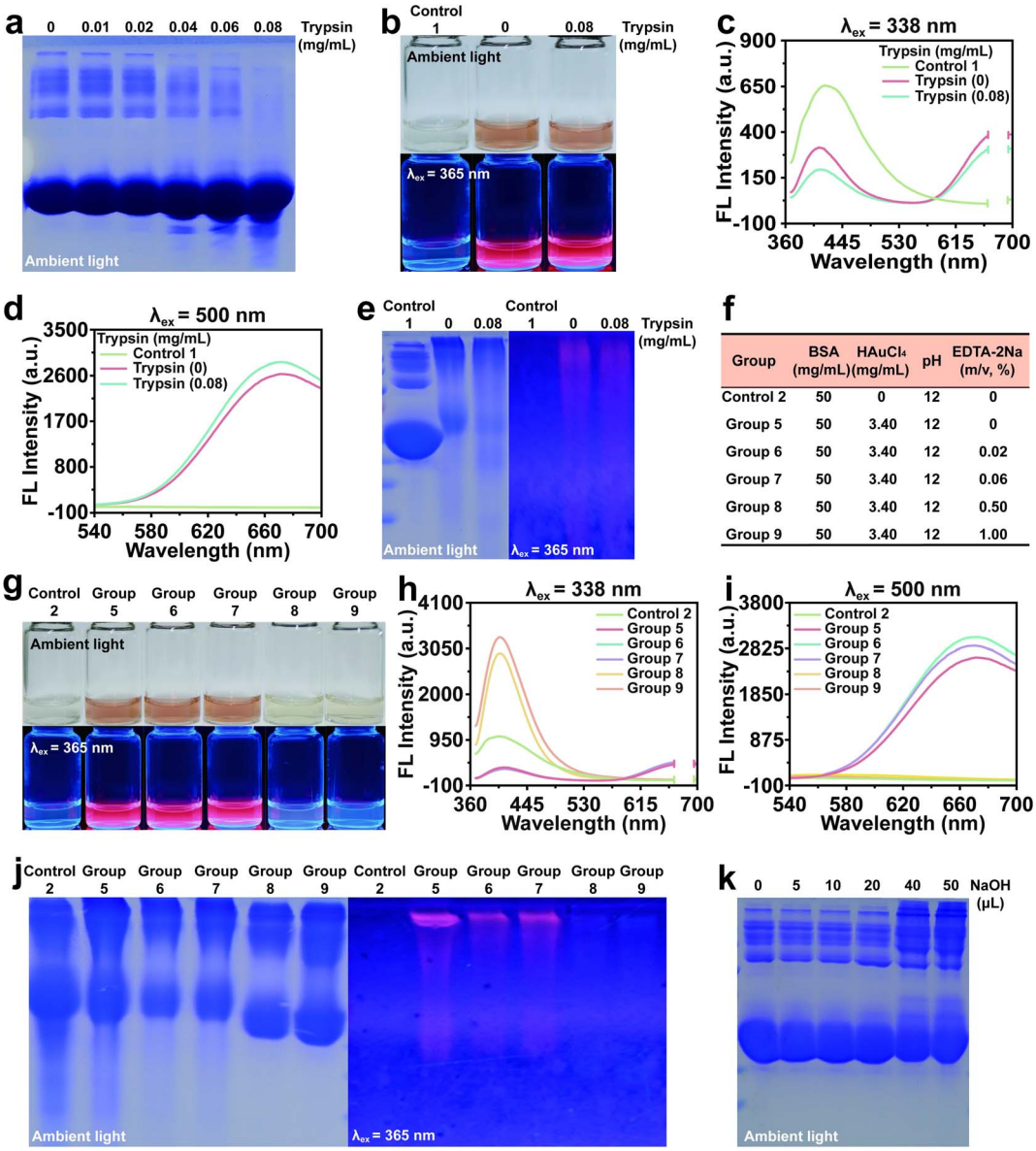

Fig. 2 The formation of BSA oligomer-stabilized Au NCs. (a) Coomassie brilliant blue staining gel image of BSA after digestion with trypsin. (b) Digital images of BSA-Au NCs digested with trypsin under ambient light (above) and 365 nm ultraviolet lamp (below). (c and d) Photoemission spectra of BSA-Au NCs digested with trypsin (λ_{ex} = 338 nm and 500 nm). (e) Coomassie brilliant blue staining gel image of BSA-Au NCs digested with trypsin (left) and Native-PAGE under 365 nm ultraviolet lamp (right). (f) BSA-Au NCs synthesized using various concentrations of EDTA-2Na. (g) Digital images of each group under ambient light (above) and 365 nm ultraviolet lamp (below). (h and i) Photoemission spectra of each group (λ_{ex} = 338 nm and 500 nm). (j) Coomassie brilliant blue staining gel image of each group (left) and Native-PAGE under 365 nm ultraviolet lamp (right). (k) Coomassie brilliant blue staining gel image of BSA treated with various volumes of NaOH (1 M). All photoemission spectra were slit widths of excitation: 5 nm, slit widths of emission: 5 nm, and voltage: 600 V.

stabilized Au NCs, which was the inherent aspect of BSA-Au NCs synthesis.

Synthesis of BSA-Au NCs at various concentrations of BSA

To further investigate the impact of BSA concentration on the synthesis of BSA-Au NCs, a fixed concentration of $HAuCl_4$ was utilized (Fig. 3a). All experimental groups exhibited red fluorescence when excited at 365 nm (Fig. 3b). Upon the introduction of Au^{3+}, it was observed that the emission intensity of each group gradually increased as the BSA concentration increased (Fig. 3c). A similar trend in fluorescence variation was also observed when excited at 500 nm, with the exception of reduced fluorescence in Group 14 (Fig. 3d). When excited at 338 nm and 500 nm, there was no significant difference of PL lifetime in Groups 10–14. The blue emission varied in the range of 4.35–4.56 ns, and the red emission varied in the range of 1.41–1.64 μs. Due to the existence of high quantum yield, the fluorescence intensity of Group 13 is the highest (Fig. S4†). The UV-vis absorption spectra indicated a decrease in absorption at 520 nm as the BSA concentration increased for each group

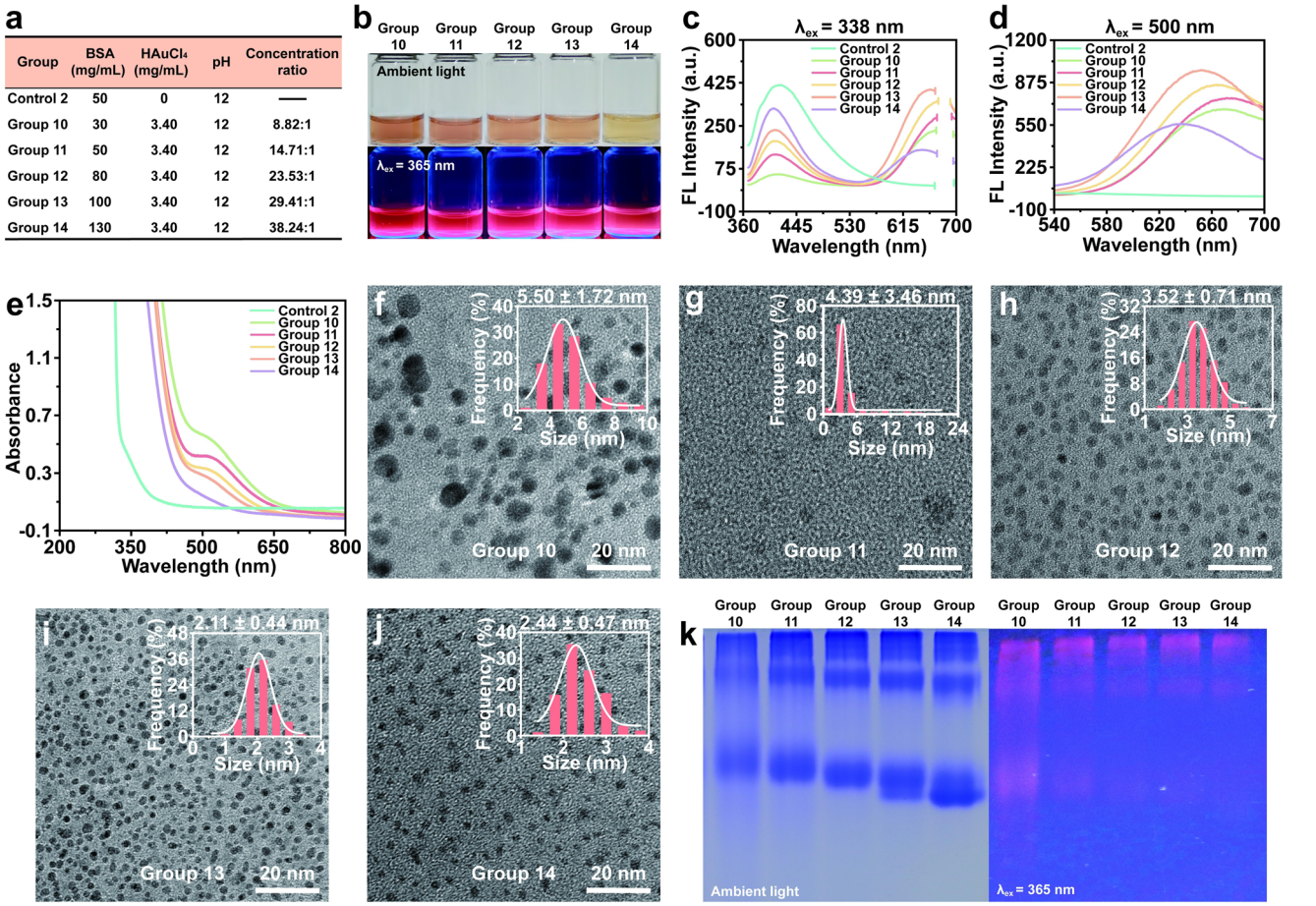

Fig. 3 Synthesis of Au NCs at various concentrations of BSA. (a) Au NCs formed at various BSA concentrations, while keeping a fixed $HAuCl_4$ concentration. (b) Digital images of each group under ambient light (above) and 365 nm ultraviolet lamp (below). (c and d) Photoemission spectra of each group (λ_{ex} = 338 nm and 500 nm). (e) UV-vis absorption spectrum of each group. (f–j) HRTEM images and particle size (inset) of each group. (k) Coomassie brilliant blue staining gel image of each group (left) and Native-PAGE under 365 nm ultraviolet lamp (right). All photoemission spectra were slit widths of excitation: 5 nm, slit widths of emission: 5 nm, and voltage: 600 V.

(Fig. 3e). To explore the potential factors contributing to the observed experimental phenomenon, we initially conducted HRTEM imaging and Native-PAGE analysis for each group (Fig. 3f–k). The obtained results indicated that the presence of a low concentration ratio led to a relative deficiency of templates, thereby facilitating the formation of larger Au NPs. Consequently, the augmentation in the absorption peak at 520 nm could be attributed to the inadequate concentration of BSA in effectively stabilizing Au atoms. As the concentration ratio increased, the synthesis of Au NPs diminished while the number of Au NCs gradually escalated. Appropriate concentration ratios could increase the amount of Au NCs and improve the quantum yield. Excitingly, Group 13 had a quantum yield of 74.3% (Table S1†). Additionally, we found that the fluorescence intensity of BSA-Au NCs exhibited minimal variation even after a storage at 4 °C for 3 months (Fig. S5†). However, when the concentration ratio was further increased to 38.24 : 1, the number of the synthesized Au NCs decreased and the heterogeneity in particle size increased. These findings indicated that the formation of BSA-Au NCs was contingent upon specific concentration ranges.

Inner filter effect

In the preceding experiments, we found that the fluorescence intensity of Group 10 was comparatively higher than that of other groups following electrophoresis, contradicting the findings of fluorescence spectroscopy. This inconsistency could be attributed to the IFE, wherein individual components in the solution competed for the absorption of excitation or emission light, resulting in a reduction in fluorescence emission intensity. Recent researches have indicated that Au NPs can effectively serve as fluorescence quenchers for the detection of target analytes by exploiting the IFE.[34,35] Hence, it was hypothesized that the presence of Au NPs in the products led to the suppression of fluorescence in the Au NCs. In order to gain a deeper understanding of this quenching mechanism, tannic acid-stabilized Au NPs were synthesized. The resulting Au NPs exhibited uniform dispersion with a particle size of 2.67 ± 0.62 nm and displayed a surface plasmon resonance absorption peak at 520 nm (Fig. 4a and b). These Au NPs were then introduced to the Au NCs emitting blue fluorescence (Group 1). The emission of Au NCs at 400 nm was significantly diminished in

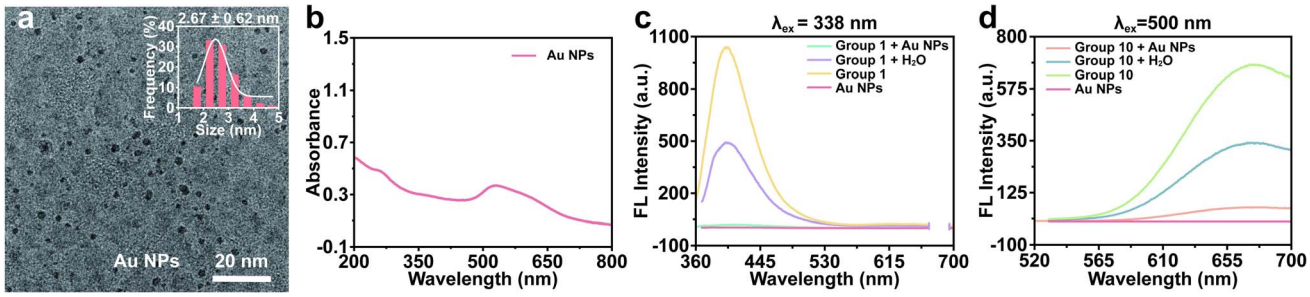

Fig. 4 Inner filter effect. (a) HRTEM images and particle size (inset) of Au NPs. (b) UV-vis absorption spectrum of Au NPs. (c) Photoemission spectra of Group 1 after adding Au NPs (λ_{ex} = 338 nm). (d) Photoemission spectra of Group 10 after adding Au NPs (λ_{ex} = 500 nm). All photoemission spectra were slit widths of excitation: 5 nm, slit widths of emission: 5 nm, and voltage: 600 V.

comparison to the control group (Fig. 4c). The addition of Au NPs to the product synthesized by Group 10 was also conducted in order to observe the potential decrease in red fluorescence. As anticipated, the red fluorescence of Au NCs was found to be partially quenched (Fig. 4d). These results indicated that Au NPs possessed the ability to effectively absorb blue fluorescence and partially absorb red fluorescence within the solution of Au NCs, owing to the existence of the IFE.

Synthesis of BSA-Au NCs at various concentrations of Au^{3+}

In order to investigate the influence of Au^{3+} on the synthesis of BSA-Au NCs, the concentration of BSA was held constant (Table S2†). It was observed that the color of the reaction system deepened with the increase of $HAuCl_4$ concentration. Only Group 15 emitted blue fluorescence, while Group 16 and Group 17 emitted blue and red fluorescence. In contrast, Group 18 and Group 19 predominantly emitted red fluorescence (Fig. S6 and S7†). In Groups 15–19, there was no significant change in PL lifetime in blue and red emission (Fig. S8†). HRTEM results revealed that the size of Au NCs decreased as the concentration ratio of BSA to Au^{3+} increased. Beyond a certain concentration ratio, Au NPs were synthesized (Fig. S9†). Native-PAGE results demonstrated that the electrophoretic mobility of the BSA-Au compounds decreased with increasing Au^{3+} concentration, indicating the formation of large Au NCs or Au NPs (Fig. S10†). These results suggested that BSA-Au NCs were synthesized only at a range of concentration ratios of BSA to Au^{3+}.

Growth mechanism of BSA-Au NCs

The changes of fluorescence were observed at various incubation times in order to investigate the correlation between the concentration of raw materials and the growth of Au NCs. Fig. 5a depicted the time-dependent fluorescent spectra of Group 1. It could be observed that as the incubation time increased, the fluorescence peak at 400 nm exhibited a gradual increase, suggesting a corresponding increase in the number of small Au NCs. The fluorescence at 400 nm was gradually decreased in Group 13, while the fluorescence at 640 nm increased during incubation (Fig. 5b and c). These results suggested that the growth of Au NCs initiated from a smaller size when the raw material concentration was low, whereas the growth of Au NCs commenced directly from a larger size when the raw material concentration was high, accompanied by noticeable alterations in fluorescence.

Hg^{2+} detection using BSA-Au NCs as fluorescent probes

We utilized Group 13 as a fluorescent probe to assess the fluorescence quenching capability of various Hg^{2+} concentrations on BSA-Au NCs at 650 nm. Fig. 6a showed that the fluorescence emission intensity was gradually decreased with the increase of Hg^{2+} concentration. When the concentration of Hg^{2+} was within the range of 0.01 to 4.5 μM, the fluorescence intensity decreased linearly, and the linear regression equation was $y = -112.46 \times x + 1129.36$ (correlation coefficients $R^2 = 0.9971$) (Fig. 6b). The limit of detection (LOD) was 0.01 μM, according to the 3σ rule. It

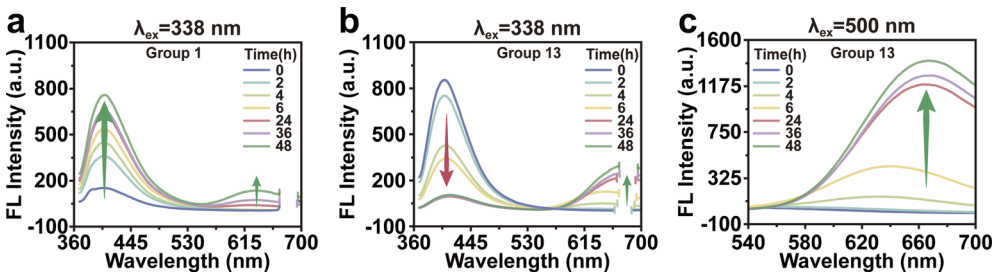

Fig. 5 Growth mechanism of BSA-Au NCs. (a) Photoemission spectra of Group 1 with time-dependent (λ_{ex} = 338 nm). (b and c) Photoemission spectra of Group 13 with time-dependent (λ_{ex} = 338 nm and 500 nm). All photoemission spectra were slit widths of excitation: 5 nm, slit widths of emission: 5 nm, and voltage: 600 V.

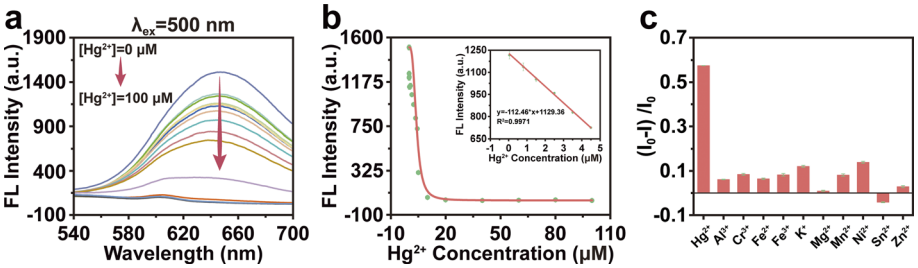

Fig. 6 Hg^{2+} detection using BSA-Au NCs as fluorescent probes. (a) Photoemission spectra of BSA-Au NCs after incubation with various concentrations of Hg^{2+} (λ_{ex} = 500 nm). Slit widths of excitation: 10 nm, slit widths of emission: 10 nm, and voltage: 700 V. (b) The fluorescence intensity changes at 650 nm. Inset: expanded linear region of the calibration curve (0.01–4.5 μM of Hg^{2+}). (c) Relative emission intensity of BSA-Au NCs after the addition of different metal ions. I_0 and I represented the emission intensity of BSA-Au NCs at 650 nm before and after the addition of metal ions, respectively.

was suggested that BSA-Au NCs could be used as a sensor with high sensitivity for Hg^{2+}. In order to evaluate the specificity of BSA-Au NCs, the dialyzed BSA-Au NCs were combined with various metal ion solutions, including K^{+}, Ni^{2+}, Fe^{3+}, Fe^{2+}, Sn^{2+}, Al^{3+}, Cr^{3+}, Mg^{2+}, Zn^{3+}, Mn^{2+}, Hg^{2+}. The fluorescence of BSA-Au NCs was predominantly quenched upon the addition of Hg^{2+} (Fig. 6c). This finding underscored the exceptional selectivity of BSA-Au NC for Hg^{2+} in contrast to other metal ions.

Conclusion

In this work, we aimed to assess the influence of BSA concentration in combination with Au^{3+} on the synthesis of BSA-Au NCs. As the concentration of the system increased, the Au NCs transitioned from small nanoclusters to large nanoclusters, resulting in a shift in fluorescence from solely blue to a dual emission of blue and red. The alkaline environment promoted the formation of protein oligomers, which acted as ligands for the generation of large Au NCs. Based on these findings, separate adjustments were made to the concentrations of BSA and Au^{3+}. Our results revealed that both BSA and Au^{3+} played a crucial role in the synthesis of BSA-Au NCs, leading to the conversion of fluorescence during growth. The intensity of fluorescence emission in the solution was reduced due to the IFE effect. We also found that the resulting Au NCs exhibited uniform particle size, notable photoluminescence properties and favorable biological stability when the concentration ratio reached its optimal value Hg^{2+}, a hazardous heavy metal, is prevalent in air, food, water, and various substances. Mercury poisoning can result in Minamata disease, limb pain, and Alzheimer's disease and other diseases that seriously threaten human life.[36] Hence, the development of efficient and sensitive Hg^{2+} detection methods holds crucial importance in safeguarding human health. Our BSA-Au NCs were used as efficient fluorescence sensors for detecting Hg^{2+} and exhibited high sensitivity and specificity.

These attributes make it a suitable nano-platform for future explorations on Au NCs, thereby expanding their potential applications in various fields. Additionally, the findings will be applicable to other reaction systems involving the presence of proteins and precious metals. The growing interest in research focused on Au NCs will undoubtedly promote extensive investigation of these nano-fluorescent materials and generate numerous interdisciplinary interests.

Conflicts of interest

There are no conflicts to declare.

Acknowledgements

This study was supported by the project funded by China Postdoctoral Science Foundation (2023MD734126), Chongqing Municipal Postdoctoral Science Special Foundation (2022CQBSHTB3003) and Chongqing Rongchang Medical Scientific Research Project (2023RCMSXM007). We would like to express our gratitude to all those who supported the subject.

References

1 E. Pomerantseva, F. Bonaccorso, X. Feng, Y. Cui and Y. Gogotsi, Energy Storage: The Future Enabled by Nanomaterials, *Science*, 2019, **366**(6468), eaan8285, DOI: 10.1126/science.aan8285.

2 Y. Zheng, L. Lai, W. Liu, H. Jiang and X. Wang, Recent Advances in Biomedical Applications of Fluorescent Gold Nanoclusters, *Adv. Colloid Interface Sci.*, 2017, **242**, 1–16, DOI: 10.1016/j.cis.2017.02.005.

3 X. Qu, Y. Li, L. Li, Y. Wang, J. Liang and J. Liang, Fluorescent Gold Nanoclusters: Synthesis and Recent Biological Application, *J. Nanomater.*, 2015, **2015**, 1–23, DOI: 10.1155/2015/784097.

4 Z. F. Pu, J. Peng, Q. L. Wen, Y. Li, J. Ling, P. Liu and Q.-E. Cao, Photocatalytic Synthesis of BSA-Au Nanoclusters with Tunable Fluorescence for Highly Selective Detection of Silver Ion, *Dyes Pigm.*, 2021, **193**, 109533, DOI: 10.1016/j.dyepig.2021.109533.

5 N. Yan, N. Xia, L. Liao, M. Zhu, F. Jin, R. Jin and Z. Wu, Unraveling the Long-Pursued Au $_{144}$ Structure by x-Ray Crystallography, *Sci. Adv.*, 2018, **4**(10), eaat7259, DOI: 10.1126/sciadv.aat7259.

6 J. Xie, Y. Zheng and J. Y. Ying, Protein-Directed Synthesis of Highly Fluorescent Gold Nanoclusters, *J. Am. Chem. Soc.*, 2009, **131**(3), 888–889, DOI: **10.1021/ja806804u**.

7 J. M. Dixon and S. Egusa, Conformational Change-Induced Fluorescence of Bovine Serum Albumin–Gold Complexes, *J. Am. Chem. Soc.*, 2018, **140**(6), 2265–2271, DOI: **10.1021/jacs.7b11712**.

8 Y. Negishi, N. K. Chaki, Y. Shichibu, R. L. Whetten and T. Tsukuda, Origin of Magic Stability of Thiolated Gold Clusters: A Case Study on $Au_{25}(SC_6H_{13})_{18}$, *J. Am. Chem. Soc.*, 2007, **129**(37), 11322–11323, DOI: **10.1021/ja073580+**.

9 Y. Shichibu, Y. Negishi, H. Tsunoyama, M. Kanehara, T. Teranishi and T. Tsukuda, Extremely High Stability of Glutathionate-Protected Au25 Clusters Against Core Etching, *Small*, 2007, **3**(5), 835–839, DOI: **10.1002/smll.200600611**.

10 Z. Tang, F. Chen, D. Wang, D. Xiong, S. Yan, S. Liu and H. Tang, Fabrication of Avidin-Stabilized Gold Nanoclusters with Dual Emissions and Their Application in Biosensing, *J. Nanobiotechnol.*, 2022, **20**(1), 306, DOI: **10.1186/s12951-022-01512-8**.

11 Y. Guo, H. T. N. N. Amunyela, Y. Cheng, Y. Xie, H. Yu, W. Yao, H.-W. Li and H. Qian, Natural Protein-Templated Fluorescent Gold Nanoclusters: Syntheses and Applications, *Food Chem.*, 2021, **335**, 127657, DOI: **10.1016/j.foodchem.2020.127657**.

12 H. Li, W. Zhu, A. Wan and L. Liu, The Mechanism and Application of the Protein-Stabilized Gold Nanocluster Sensing System, *Analyst*, 2017, **142**(4), 567–581, DOI: **10.1039/c6an02112c**.

13 M. Zhu, C. M. Aikens, F. J. Hollander, G. C. Schatz and R. Jin, Correlating the Crystal Structure of a Thiol-Protected Au25 Cluster and Optical Properties, *J. Am. Chem. Soc.*, 2008, **130**(18), 5883–5885, DOI: **10.1021/ja801173r**.

14 H. Kawasaki, K. Hamaguchi, I. Osaka and R. Arakawa, Ph-Dependent Synthesis of Pepsin-Mediated Gold Nanoclusters with Blue Green and Red Fluorescent Emission, *Adv. Funct. Mater.*, 2011, **21**(18), 3508–3515, DOI: **10.1002/adfm.201100886**.

15 Q. Yao, X. Yuan, T. Chen, D. T. Leong and J. Xie, Engineering Functional Metal Materials at the Atomic Level, *Adv. Mater.*, 2018, **30**(47), e1802751, DOI: **10.1002/adma.201802751**.

16 Y. Tao, M. Li, J. Ren and X. Qu, Metal Nanoclusters: Novel Probes for Diagnostic and Therapeutic Applications, *Chem. Soc. Rev.*, 2015, **44**(23), 8636–8663, DOI: **10.1039/C5CS00607D**.

17 F. Xia, A. He, H. Zhao, Y. Sun, Q. Duan, S. J. Abbas, J. Liu, Z. Xiao and W. Tan, Molecular Engineering of Aptamer Self-Assemblies Increases *in Vivo* Stability and Targeted Recognition, *ACS Nano*, 2022, **16**(1), 169–179, DOI: **10.1021/acsnano.1c05265**.

18 Y. Chen, Y. Wang, C. Wang, W. Li, H. Zhou, H. Jiao, Q. Lin and C. Yu, Papain-Directed Synthesis of Luminescent Gold Nanoclusters and the Sensitive Detection of Cu^{2+}, *J. Colloid Interface Sci.*, 2013, **396**, 63–68, DOI: **10.1016/j.jcis.2013.01.031**.

19 N. El-Sayed, V. Trouillet, A. Clasen, G. Jung, K. Hollemeyer and M. Schneider, NIR-Emitting Gold Nanoclusters-Modified Gelatin Nanoparticles as a Bioimaging Agent in Tissue, *Adv. Healthcare Mater.*, 2019, **8**(24), e1900993, DOI: **10.1002/adhm.201900993**.

20 G. Liu, Y. Shao, K. Ma, Q. Cui, F. Wu and S. Xu, Synthesis of DNA-Templated Fluorescent Gold Nanoclusters, *Gold Bull.*, 2012, **45**(2), 69–74, DOI: **10.1007/s13404-012-0049-6**.

21 A. Maity and A. Kumar, Higher-Order Assembly of BSA Gold Nanoclusters Using Supramolecular Host-Guest Chemistry: A 40% Absolute Fluorescence Quantum Yield, *Nanoscale Adv.*, 2022, **4**(14), 2988–2991, DOI: **10.1039/d2na00123c**.

22 H. Lin, L. Li, C. Lei, X. Xu, Z. Nie, M. Guo, Y. Huang and S. Yao, Immune-Independent and Label-Free Fluorescent Assay for Cystatin C Detection Based on Protein-Stabilized Au Nanoclusters, *Biosens. Bioelectron.*, 2013, **41**, 256–261, DOI: **10.1016/j.bios.2012.08.030**.

23 P. U. P. A. Gilbert, K. D. Bergmann, N. Boekelheide, S. Tambutté, T. Mass, F. Marin, J. F. Adkins, J. Erez, B. Gilbert, V. Knutson, M. Cantine, J. O. Hernández and A. H. Knoll, Biomineralization: Integrating Mechanism and Evolutionary History, *Sci. Adv.*, 2022, **8**(10), eabl9653, DOI: **10.1126/sciadv.abl9653**.

24 Y. Xu, J. Sherwood, Y. Qin, D. Crowley, M. Bonizzoni and Y. Bao, The Role of Protein Characteristics in the Formation and Fluorescence of Au Nanoclusters, *Nanoscale*, 2014, **6**(3), 1515–1524, DOI: **10.1039/C3NR06040C**.

25 M. Yang, Z. Lian, C. Si and B. Li, Revealing the Role of Nitrogen Dopants in Tuning the Electronic and Optical Properties of Graphene Quantum Dots *via* a TD-DFT Study, *Phys. Chem. Chem. Phys.*, 2020, **22**(48), 28230–28237, DOI: **10.1039/d0cp04707d**.

26 P. L. Xavier, K. Chaudhari, P. K. Verma, S. K. Pal and T. Pradeep, Luminescent Quantum Clusters of Gold in Transferrin Family Protein, Lactoferrin Exhibiting FRET, *Nanoscale*, 2010, **2**(12), 2769–2776, DOI: **10.1039/c0nr00377h**.

27 M. E. Ali, U. Hashim, S. Mustafa, Y. B. Che Man, M. H. M. Yusop, M. Kashif, Th. S. Dhahi, M. F. Bari, M. A. Hakim and M. A. Latif, Nanobiosensor for Detection and Quantification of DNA Sequences in Degraded Mixed Meats, *J. Nanomater.*, 2011, **2011**, 1–11, DOI: **10.1155/2011/781098**.

28 Y. Liu, K. Ai, X. Cheng, L. Huo and L. Lu, Gold-Nanocluster-Based Fluorescent Sensors for Highly Sensitive and Selective Detection of Cyanide in Water, *Adv. Funct. Mater.*, 2010, **20**(6), 951–956, DOI: **10.1002/adfm.200902062**.

29 X. Wu, X. He, K. Wang, C. Xie, B. Zhou and Z. Qing, Ultrasmall Near-Infrared Gold Nanoclusters for Tumor Fluorescence Imaging in Vivo, *Nanoscale*, 2010, **2**(10), 2244, DOI: **10.1039/c0nr00359j**.

30 T. H. Chen and W. L. Tseng, (Lysozyme Type VI)-Stabilized Au8 Clusters: Synthesis Mechanism and Application for Sensing of Glutathione in a Single Drop of Blood, *Small*, 2012, **8**(12), 1912–1919, DOI: **10.1002/smll.201102741**.

31 M. Yang, C. Dutta and A. Tiwari, Disulfide-Bond Scrambling Promotes Amorphous Aggregates in Lysozyme and Bovine Serum Albumin, *J. Phys. Chem. B*, 2015, **119**(10), 3969–3981, DOI: **10.1021/acs.jpcb.5b00144**.

32 B. K. Jha, D. M. Salunke and K. Datta, Disulfide Bond Formation through Cys186 Facilitates Functionally Relevant Dimerization of Trimeric Hyaluronan-Binding Protein 1 (HABP1)/P32/gC1qR, *Eur. J. Biochem.*, 2002, **269**(1), 298–306, DOI: **10.1046/j.0014-2956.2001.02654.x**.

33 M. K. Song, X. N. Guo and K. X. Zhu, Characterization of the Alkali-Induced Protein Cross-Linking in Buckwheat Sourdough Steamed Bread, *Food Hydrocolloids*, 2023, **145**, 109143, DOI: **10.1016/j.foodhyd.2023.109143**.

34 H. C. Chang and J. A. Ho, Gold Nanocluster-Assisted Fluorescent Detection for Hydrogen Peroxide and Cholesterol Based on the Inner Filter Effect of Gold Nanoparticles, *Anal. Chem.*, 2015, **87**(20), 10362–10367, DOI: **10.1021/acs.analchem.5b02452**.

35 Y. Liu, H. Li, B. Guo, L. Wei, B. Chen and Y. Zhang, Gold Nanoclusters as Switch-off Fluorescent Probe for Detection of Uric Acid Based on the Inner Filter Effect of Hydrogen Peroxide-Mediated Enlargement of Gold Nanoparticles, *Biosens. Bioelectron.*, 2017, **91**, 734–740, DOI: **10.1016/j.bios.2017.01.020**.

36 G. Ferreira, A. Santander, L. Chavarría, R. Cardozo, F. Savio, L. Sobrevia and G. L. Nicolson, Functional Consequences of Lead and Mercury Exposomes in the Heart, *Mol. Aspects Med.*, 2022, **87**, 101048, DOI: **10.1016/j.mam.2021.101048**.